Interaction of Fusion Peptides from HIV gp41 with Membranes: A Time-Resolved Membrane Binding, Lipid Mixing, and Structural Study†

Víctor Buzón, Esteve Padrós, and Josep Cladera*

Unitat de Biofísica, Departament de Bioquímica i de Biologia Molecular, Facultat de Medicina, Universitat Autònoma de Barcelona. 08193 Bellaterra, Barcelona, Spain

Received March 1, 2005; Revised Manuscript Received June 7, 2005

ABSTRACT: The interaction of the so-called fusion peptide of the human immunodeficiency virus gp41 envelope glycoprotein with the target cell membrane is believed to trigger the fusion process which allows the entry of the virus into the cell. Many studies on the interaction of the fusion peptide with biological membranes have been carried out using synthetic peptides and model membranes. Due to the variety of experimental systems and sequences used, some controversy exists, concerning mainly the type of structure which triggers membrane destabilization and fusion (α helix or β structure). With the aim of contributing to shed some light on the subject we have undertaken a series of experiments on the interaction of the three most representative fusion sequences with model membranes under the same experimental conditions. The results show that the fusion peptides, which adopt an unordered structure when dissolved in DMSO, form a mixture of aggregated β and helical + unordered structures in aqueous buffer. Model membranes are shown to enhance the formation of aggregated β structures. The nature of the membrane binding event, the kinetics of the binding and lipid mixing processes, and the kinetics of the structural changes depend on whether both ends of the fusion sequence or just one bears a positive charge. Analysis of the kinetic data shows that lipid mixing depends on the transformation of unordered + helical structures into aggregated β structures upon binding to the membrane.

According to a nowadays widely accepted hypothesis, human immunodeficiency virus (HIV-1)[1] entry into the target cell is triggered by the interaction of the viral glycoprotein gp41 with the cell membrane (*1*−*6*). In the viral envelope gp41 is noncovalently associated to gp120, the glycoprotein responsible for T-lymphocyte recognition. Following the interaction of gp120 with the CD4 receptor and various coreceptors on the cell membrane, a series of conformational rearrangements takes place, which results in the interaction of the N-terminal part of gp41 with the cell membrane. This process has been described to trigger the fusion of the viral and the cellular membranes, and the involvement of the 23 N-terminal fragment (the fusion peptide) of gp41 has been deduced from mutagenesis experiments, which have shown the importance of different residues within the segment for the fusion event to take place (*7*−*11*). gp41 has been crystallized, and it has been shown to form a trimeric structure composed of three coiled α helices (*12*−*14*), a conformation that was first described for influenza's hemagglutinin (*15*) and that has been proposed for the fusion proteins of other viruses (*2*). A general model, the so-called "spring loaded mechanism" (*16*), by which the viral fusion protein makes contact with the target cell membrane and causes the viral and cellular membranes to become close enough for membrane fusion to occur, has been elaborated from the above-mentioned structural studies. The structures deduced from the diffraction data, however, are devoid of the N-terminal fusion peptide, since its hydrophobicity makes necessary its removal in order to get the protein crystals. Nevertheless, a considerable amount of structural and functional data has been gathered in the past decade from experiments using synthetic peptides with sequences corresponding to different lengths of the N-terminal fusion peptide of mainly influenza but also HIV and other viruses (*17*−*40*). In the case of immunodeficiency viruses, the interpretation of the experimental results has resulted in two different and contradictory views on the structure adopted by the fusion peptide upon interaction with model membranes and its importance for the membrane fusion process. Data from Nieva's laboratory (*27*−*32*, *40*) for example, obtained from studies with a 23 residue long fusion peptide, indicate that the fusogenic conformation corresponds to a β-pleated structure which absorbs in the infrared region characteristic for proteinaceous aggregates. Formation of β-pleated structure upon membrane interaction has been detected as well by Weliky and collaborators (*35*, *36*, *41*−*43*). On the other hand, working with a 16 residue long sequence, Ruysschaert's group in Brussels have reported the formation of an obliquely inserted α helix in the membrane, which would

† This work was funded by "Fundació La Marató de TV3" (Project Ref. 020410) (J.C.).

* Corresponding author. E-mail: josep.cladera@uab.es. Phone: 00-34-935812112. Fax: 00-34-935811907.

[1] Abbreviations: HIV-1, human immunodeficiency virus type-1; PC, phophatidylcholine; PE, phosphatidylethanolamine; DMSO, dimethyl sulfoxide; FPE, fluorescein-phosphatidylethanolamine; Rh-PE, *N*-(lissamine rhodamine B sulfonyl) phosphatidylethanolamine; NBD-PE, *N*-(nitrobenzo-2-oxa-1,3-diazol) phosphatidylethanolamine; ANTS, 8-aminonaphthalene-1,3,6-trisulfonic acid, disodium salt; DPX, *p*-xylene-bis-pyridinium bromide; FP, fusion peptide; LUVs, large unilamellar vesicles; FTIR, Fourier transform infrared; gp41, glycoprotein 41; gp120, glycoprotein 120; FRET, fluorescence resonance energy transfer.

10.1021/bi050382r CCC: $30.25
Published on Web 09/16/2005

trigger the destabilization of the lipidic bilayer and the fusion process (*21*−*26*, *33*). Differences in the length of the sequences used, composition of the model membranes, and other experimental parameters make it difficult to draw clear conclusions from the comparison of the different studies. On the other hand, the structural studies describe the conformation of the peptides at the end of the fusion process or in other nonfusogenic conditions. Information on the structure of the fusion peptides during the membrane fusion process is lacking.

In the present work we have studied the interaction of the two most widely used HIV fusion domain sequences (16 and 23 residue long sequences) with model membranes in the same experimental conditions, with the aim of getting and comparing information on the kinetics of the structural changes, the membrane binding, and the lipid mixing processes. Phosphatidylcholine/phosphatidylethanolamine (1:1) membranes have been chosen as model membranes. Phosphatidylethanolamine (PE) is together with phosphatidylcholine (PC), cholesterol, sphingomyelin, and phosphatidylserine (PS) one of the major lipidic components of the viral membrane (*44*). PE as a nonlamellar lipid has been described as a generator of negative curvature in the bilayer and a modulator of the tendency of bilayers to fuse (*38*). Most of the works in which helicoidal structures are presented as the ones responsible for triggering the fusion process have been carried out using PC/PE membranes (*21*, *24*). Finally, using PC/PE membranes we attempt to define a basic lipid system that could be supplemented with other components (cholesterol, PS, sphingomyelin) in order to study systematically their importance in subsequent works.

The results show that lipid mixing depends on the transformation of unordered and probably helical structures into aggregated β structures and that such a conformational change occurs upon binding to the membrane. Moreover the kinetics of the process greatly depend on whether the two ends of the peptidic sequence or just one of them bears a positive charge.

MATERIALS AND METHODS

Materials. Egg phophatidylcholine, egg phosphatidylethanolamine, and Triton X-100 were purchased from Sigma Chemical Company. Fluorescein-phospahtidylethanolamine, *N*-(lissamine rhodamine B sulfonyl) phosphatidylethanolamine, *N*-(nitrobenzo-2-oxa-1,3-diazol) phosphatidylethanolamine, 8-aminonaphthalene-1,3,6-trisulfonic acid, disodium salt (ANTS), and *p*-xylene-bis-pyridinium bromide (DPX) were purchased from Molecular Probes Inc. Deuterated dimethyl sulfoxide was purchased from Merck. All others reagents were of analytical grade.

Peptide Synthesis. The sequences corresponding to the N-terminus of the HIV-1 gp41 were synthesized using chloride as a counterion and purified (estimated homogeneity >90%) by Jerini Peptide Technologies. Peptide stock solutions were prepared in deuterated dimethyl sulfoxide (spectroscopy grade). The sequences used were as follows:

FP16: H-AVGIGALFLGFLGAAG-$CONH_2$

FP23-Ac: Ac-AVGIGALFLGFLGAAGSTMGARS-$CONH_2$

FP23-H: H-AVGIGALFLGFLGAAGSTMGARS-$CONH_2$

Vesicle Preparation and Labeling with Fluorescein-phosphatidylethanolamine. Large unilamellar lipid vesicles were prepared according to Mayer et al. (*45*). Phospholipids (phosphatidylcholine and phosphatidylethanolamine 1:1) dissolved in chloroform were mixed in a round-bottom flask, and the solution was dried under a stream of nitrogen until a thin film was obtained. The film was resuspended in buffer (10 mM Tris pH 7.5 for fluorescence experiments or 10 mM Hepes pD 7.5 for infrared measurements) and then frozen and thawed 5 times. Finally the vesicle suspension was extruded 10 times through 2 polycarbonate filters of pore size 100 nm using a LiposoFast extruder. The vesicles were labeled exclusively in the outer bilayer leaflet with FPE as described by Wall et al. (*46*). Briefly, LUVs were incubated with 0.25 mol % FPE dissolved in ethanol (never more than 0.1% of the total aqueous volume) at 37 °C for 1 h in the dark. Any remaining unincorporated FPE was removed by gel filtration on a PD10 Sephadex G-25 column equilibrated with the appropriate buffer. FPE-vesicles were stored at 4 °C until use in an oxygen-free atmosphere.

Fluorescence Measurements with FPE-Labeled Membranes. Fluorescence time courses of FPE-labeled vesicles were measured after the desired amount of peptide was added into 2 mL of lipid suspensions (300 μM lipid) with an SLM-Aminco 8000 spectrofluorimeter. Excitation and emission wavelengths were set at 490 and 520 nm, respectively. Temperature was controlled with a thermostatic bath at 20 °C. The contribution of light scattering to the fluorescence signals was measured in experiments without the dye and was subtracted from the fluorescence traces. Data were fitted either to a hyperbolic or to a sigmoidal binding model (*47*) respectively using the equations

$$F = (F_{max}[FP])/(K_d + [FP]) \quad (1)$$

$$F = (F_{max}[FP])^n/(K_d{}^n + [FP])^n \quad (2)$$

where F is the fluorescence variation, F_{max} the maximum fluorescence variation, [FP] the fusion peptide concentration, K_d the dissociation constant of the membrane binding process, and n the Hill coefficient. The experimental points shown in the figures are the mean values of two measurements.

Lipid Mixing Measurements. Lipid mixing experiments were carried out by measuring the fluorescence intensity change resulting from the fluorescence resonance energy transfer between NBD-PE and Rh-PE, inserted into the lipid bilayer, as described by Struck et al. (*48*). Fluorescence was monitored by using an SLM-Aminco 8000 spectrofluorimeter. Vesicles were prepared as described above, but in this case the dyes were added into the initial organic lipid solution. Vesicles containing both dyes at 0.6 mol % each were mixed with dye-free vesicles (1:9 molar ratio) at a final lipid concentration of 300 μM. The initial fluorescence of the labeled/unlabeled vesicle suspension was taken as 0% lipid mixing, and the 100% lipid mixing was determined by adding Triton X-100 at a final concentration of 0.1% (v/v). The excitation wavelength was 465 nm and emission wavelength 530 nm. Temperature was controlled with a thermostatic bath at 20 °C. The experimental points shown in the figures are the mean values of two measurements.

Leakage Measurements. For leakage experiments, release of vesicle contents to the medium induced by addition of

different fusion peptides was monitored using the ANTS/DPX assay (*49*). LUVs (50 μM) containing 12.5 mM ANTS, 45 mM DPX, 20 mM NaCl, and 10 mM Tris pH 7.5 were separated from unencapsulated material by gel filtration in a PD10 Sephadex G-25 column equilibrated with the appropriate buffer and eluted with 10 mM Tris, 100 mM NaCl pH 7.5. Fluorescence measurements were recorded with an SLM-Aminco 8000 spectrofluorimeter. Excitation and emission wavelengths of ANTS were set at 353 and 520 nm, respectively. Temperature was controlled with a thermostatic bath at 20 °C. Fluorescence of the vesicles at time zero was taken as 0% fluorescence, and the 100% fluorescence value was obtained by adding Triton X-100 (0.5% v/v).

Vesicle's *Size Measurements.* PC/PE (1:1) liposomes were incubated overnight at room temperature with the fusion peptides at different lipid-to-peptide ratios. Vesicle size distributions were measured by dynamic light scattering, using an ultrafine particle analyzer (UPA) 150 (Microtrac, Montgomeryville, PA). All parameters were fixed as previously described (*50*).

Fourier Transform Infrared Spectroscopy (FTIR) Measurements. FTIR spectra were recorded at 20 °C on an FTIR-Mattson Polaris spectrometer, equipped with a cooled liquid nitrogen mercury−cadmium−telluride (MCT) detector, at a nominal resolution of 2 cm^{-1}. The spectrometer was continuously purged with dry air (dew point lower than −60 °C). All spectra were corrected for atmospheric water vapor contribution. For time-resolved experiments vesicles from stock solutions in deuterated Hepes buffer and peptides from stock solutions in deuterated DMSO were mixed at different lipid-to-peptide ratios and immediately placed between two CaF_2 windows separated with a 50 μm spacer. Ten scans were collected and averaged using the shuttle device every 80 s for 30 min. Spectra of the peptides in deuterated DMSO were collected by placing the peptide dissolved in pure DMSO between the windows and averaging 400 scans using the shuttle device after incubation in the solvent for at least a half-hour. Concentration of the peptides for FTIR experiments was always around 1 mM. FTIR spectra for the analysis of the ester carbonyl region were collected by placing a PC/PE vesicle suspension in deuterated buffer (10 mM lipid) or a mixture of PC/PE vesicles (10 mM) and fusion peptide (1 mM, incubated overnight with the lipid) between the two CaF_2 windows separated by a 50 μm spacer. Four hundred scans were averaged using the shuttle accessory. Solvent contributions were always subtracted form the spectra.

Mathematical Fitting of Experimental Traces. Fluorescence variation traces (from membrane binding and lipid mixing experiments) and FTIR time-resolved data were fitted to exponential processes using the following equation:

$$\text{single exponential:} \quad y = y_0 - A_1 e^{-k_{app}t} \tag{3}$$

$$\text{double exponential:} \quad y = y_0 - A_1 e^{-k_{app1}t} - A_2 e^{-k_{app2}t} \tag{4}$$

where A is the amplitude of the exponential process, k_{app} its the apparent rate constant, and t is time.

RESULTS

Aggregation State and Secondary Structure of the Fusion Peptides in DMSO. The infrared transmission spectrum of the 16 residue long fusion peptide FP16 dissolved in DMSO is shown in Figure 1. The spectrum of the peptide in the amide I region was obtained after subtracting the spectral contributions from DMSO, as illustrated in the figure inset. FP16 in DMSO shows an IR absorption maximum at 1666 cm^{-1}. Such an amide I maximum has been assigned by Jackson and Mantsch (*51*), for proteins and peptides dissolved in DMSO, to the stretching vibration of amide carbonyls which do not form hydrogen bonds with the amide NH groups. In these conditions carbonyls would be substituted as hydrogen bond acceptors by the SO groups from DMSO. The authors infer, in a study with different proteins and peptides, that the polypeptidic chains are unaggregated and unstructured when dissolved in pure DMSO. Infrared spectra similar to those shown in Figure 1 were obtained in the present work for the fusion peptides FP23-H and FP23-Ac (not shown). The fusion peptides in pure DMSO are, therefore, monomeric and unstructured, according to their IR spectra.

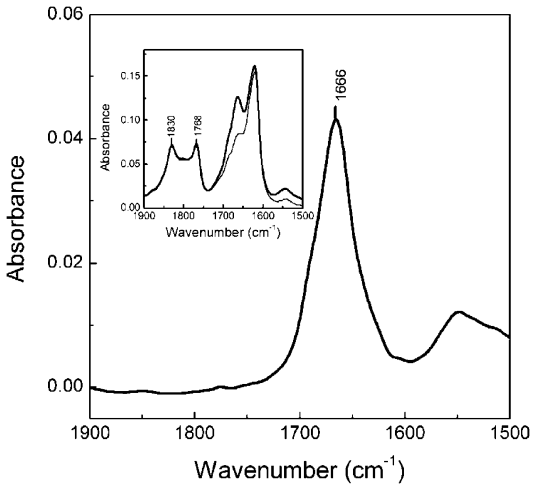

FIGURE 1: Fourier transform infrared spectra of FP16 in DMSO. The amide I and II regions are shown, after subtracting the spectrum of the pure solvent from the spectrum of the sample. The inset shows both spectra before the subtraction. Bands at 1830 and 1788 cm^{-1} correspond to DMSO and have been used as the factoring reference for the subtraction. Temperature 20 °C. Four hundred scans were acquired and averaged for every spectrum. Spectra shown are representative of two different measurements.

Binding of the Fusion Peptides to Model Membranes. Binding of the fusion peptides to the PC/PE (1:1) model membranes was monitored using the electrostatic surface potential sensor FPE (0.25 mol %) (*52*, *53*). The change in the magnitude of the surface potential, as a consequence of the interaction of the positive charges with the membrane surface, resulted in an increase of the fluorescence of the FPE dye, which is inserted in the membrane leaving the fluorophore at the membrane surface (Figure 2A). The binding curves shown in Figure 2B represent the fluorescence change as a function of peptide concentration for the three sequences. The binding curve corresponding to FP16 is consistent with the one previously published using the same technique (*54*), showing a clear interaction of the peptide with the membrane surface, with a dissociation constant of ca. 10 μM. The binding curve of FP23-Ac follows a very similar pattern. In both cases the binding curves have a predominant hyperbolic character (eq 1) with no significant signs of sigmoidality. Binding of FP23-H, however, gives a

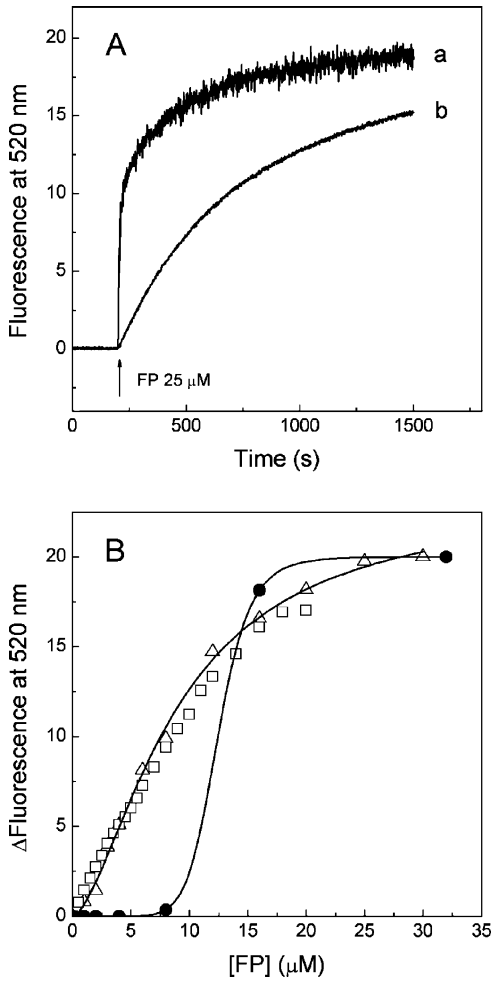

FIGURE 2: Binding of the fusion peptides to the PC/PE (1:1) model membranes. (A) FPE fluorescence variation as a function of time upon peptide addition (25 μM) to the PC/PE (1:1) membrane suspension: (a) FP23-Ac (FP16 gave a very similar trace); (b) FP23-H. The fluorescence traces shown are representative of two independent experiments. (B) The amplitude of the fluorescence variation as a function of peptide concentration was used to obtain the binding curves: FP16 (triangles), FP23-Ac (squares), and FP23-H (full circles). The amplitude of fluorescence variation was measured when the traces shown in A reached a plateau, ca. 3000 s. The solid lines are the best fits using eq 1 for FP16 and FP23-Ac and eq 2 for FP23-H. Each experimental point is the average of two independent measurements. Lipid concentration was 300 μM. Temperature 20 °C. The buffer was 10 mM Tris pH 7.5

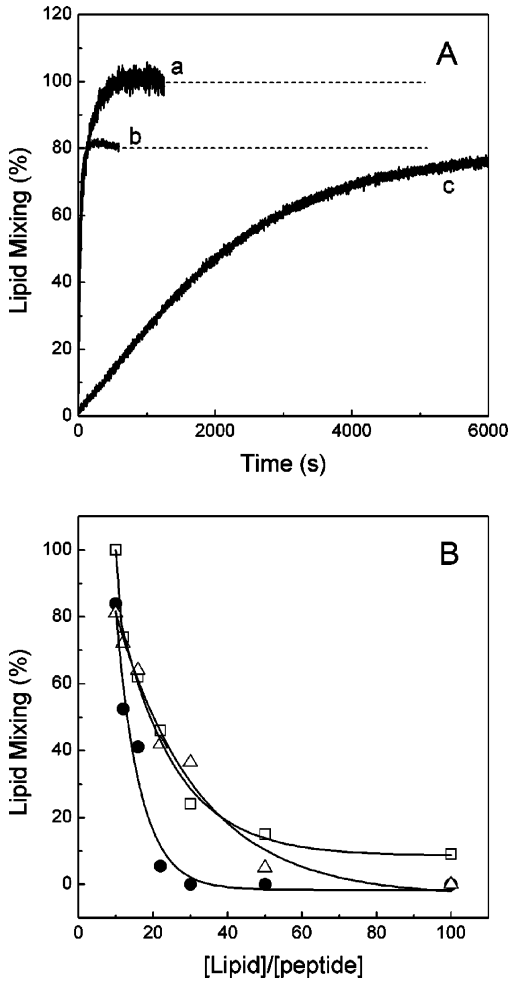

FIGURE 3: (A) Lipid mixing time course caused by addition of 25 μM FP23-Ac (a), FP16 (b), and FP23-H (c) to a 300 μM PC/PE (1:1) membrane suspension. (B) Percentage of lipid mixing as a function of the lipid/peptide ratio: FP16 (triangles), FP23-Ac (squares), and FP23-H (full circles). The amplitude of fluorescence variation was measured when the traces shown in A reached a plateau (ca. 1000 s for a and b, ca. 10000 s for c). Temperature 20 °C. Fluorescence traces in A are representative of two independent measurements, and each data point in B is the average of two experiments. The buffer was 10 mM Tris pH 7.5

clearly sigmoidal binding curve, with a Hill coefficient of 9 and a dissociation constant ca. 12 μM, calculated using eq 2.

Lipid Mixing. The peptides' fusogenic capacity was monitored by measuring their ability to induce lipid mixing in model membrane vesicle suspensions.

FRET measurements were carried out using the dyes Rhodamine and NBD according to Struck et al. (*48*). Figure 3A shows the increase in fluorescence intensity of NBD (decrease in energy transfer) as a consequence of the lipid mixing and dye dilution caused by the addition of the fusion peptides. The results clearly show that, whereas the addition of both FP16 and FP23-Ac produced very similar kinetics, addition of FP23-H caused a much slower lipid mixing process. In Figure 3B the extent of lipid mixing has been plotted against the lipid/peptide ratio for the three fusion sequences: FP23-Ac and FP16 caused very similar extents of lipid mixing at the same lipid/peptide ratios, but lower ratios are sufficient to attain the same levels when using FP23-H.

Structural Changes upon Peptide-Membrane Interaction. To gain insight on the kinetics of the conformational changes taking place during the membrane binding and lipid mixing processes, we monitored the secondary structure variations of the fusion peptides as a function of time in the absence and presence of membranes, using transmission FTIR. The results are summarized in Figure 4. The spectra corresponding to the FP23-H sequence when added into the buffer (Figure 4A) reveal two main bands: one centered at 1624 cm^{-1}, characteristic of aggregated intermolecular β structures (*23*, *28*), and another with a maximum between 1645 and 1648 cm^{-1}, which according to the usual assignments found in the literature for spectra in D_2O suspensions would correspond to a mixture of unordered and helical structures (*55*). From the relative intensities of both bands it can be roughly estimated that the FP23-H peptide forms in water molecular aggregates composed of a mixture of intermolecular β structures and unordered + helical structures. When

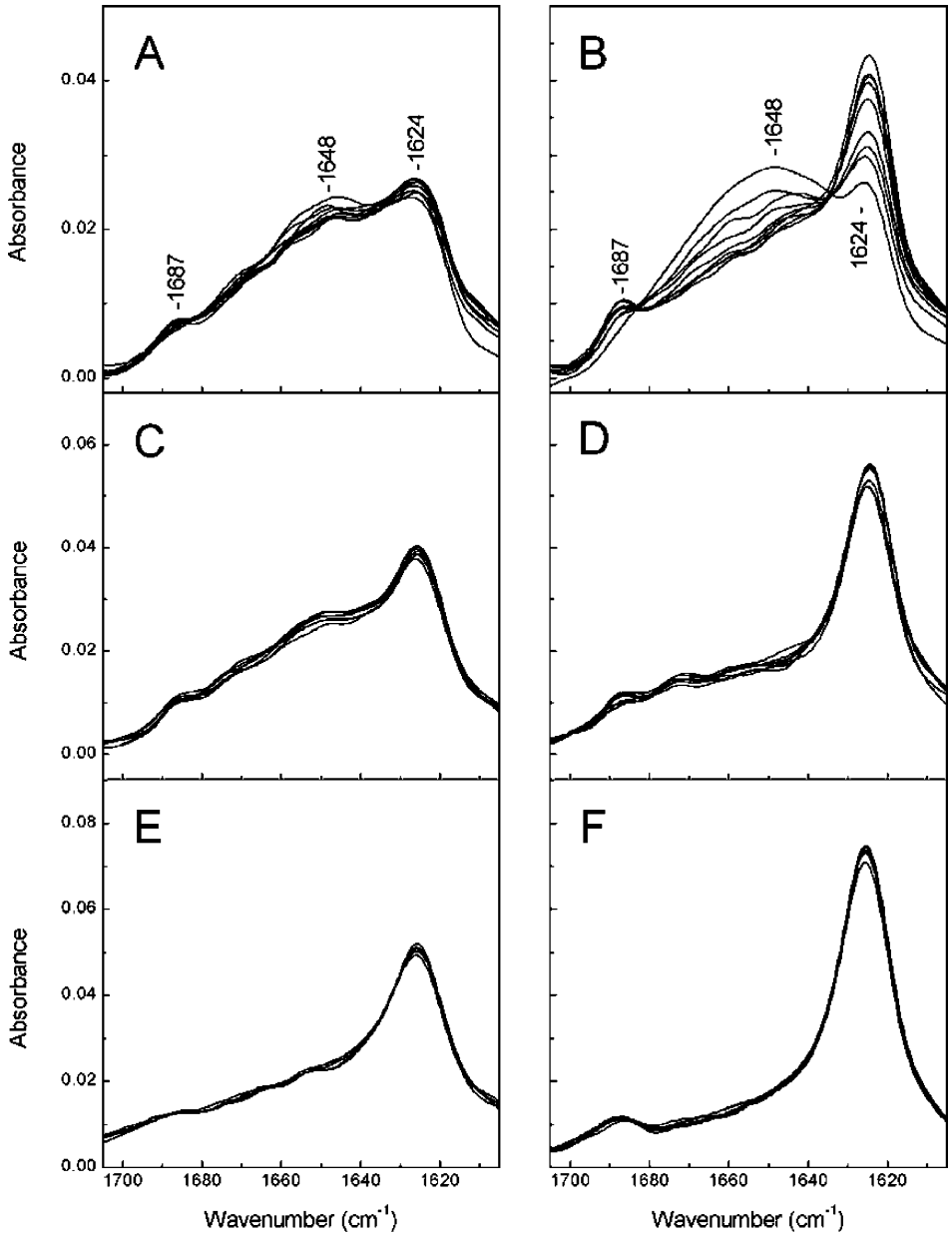

FIGURE 4: Effect of the addition of the fusion peptide (1 mM) into deuterated 10 mM Hepes buffer (A, C, E) and to a 10 mM PC/PE (1:1) membrane suspension in the same buffer (B, D, F) measured by transmission FTIR. Spectra acquired as a function of time are shown for FP23-H (A, B), FP23-Ac (C, D), and FP16 (E, F). Each spectrum is the average of 10 scans, and the spectral contribution of the buffer was always subtracted. One spectrum was collected every 80 s. Temperature 20 °C. pD 7.5. The series of spectra shown are representative of two independent measurements.

the FP23-Ac sequence is mixed with the aqueous buffer (Figure 4C), the infrared spectra reveal the same structural components as for FP23-H, but in this case the amount of unordered + helical structures is reduced in favor of the intermolecular β aggregates. This effect is clearly more intense when FP16 in added into Hepes buffer (Figure 4E): the feature which dominates the infrared spectra is then the band at 1624 cm^{-1}, whereas there is only a residual component at 1645−50 cm^{-1}.

On the other hand, when the peptides were mixed with PC/PE model membranes (Figure 4B,D,F) it becomes apparent that a larger amount of aggregated β structure did form, as compared with the spectra of the peptides in water, at the same peptide concentration.

For FP23-H (Figure 4B), we have been able to measure this β structure formation as an increment of the absorbance at 1624 cm^{-1}, which is simultaneous with the disappearance of a broad band centered at 1648 cm^{-1}. This broad band, detected just 50 s after the peptide was mixed with the membranes, can be again interpreted as being the result of a mixture of spectral components assignable to helical (α helices and polyproline II type helices) and unordered structures (*47*, *56*, *57*). In the case of FP3-Ac (Figure 4D) and FP16 (Figure 4F), the sequences of FTIR spectra measured show that the formation of the β structure as a consequence of mixing the peptides with the membranes is a faster process. As with FP23-H it is possible that helical structures (absorbing at 1648 cm^{-1}) do form within the dead time (approximately 50 s) of our measuring procedure.

In Figure 5 the absorbance increment at 1624 cm^{-1} reported in Figure 4 with respect to the absorbance measured at 1648 cm^{-1} is plotted as a function of time. For FP23-H

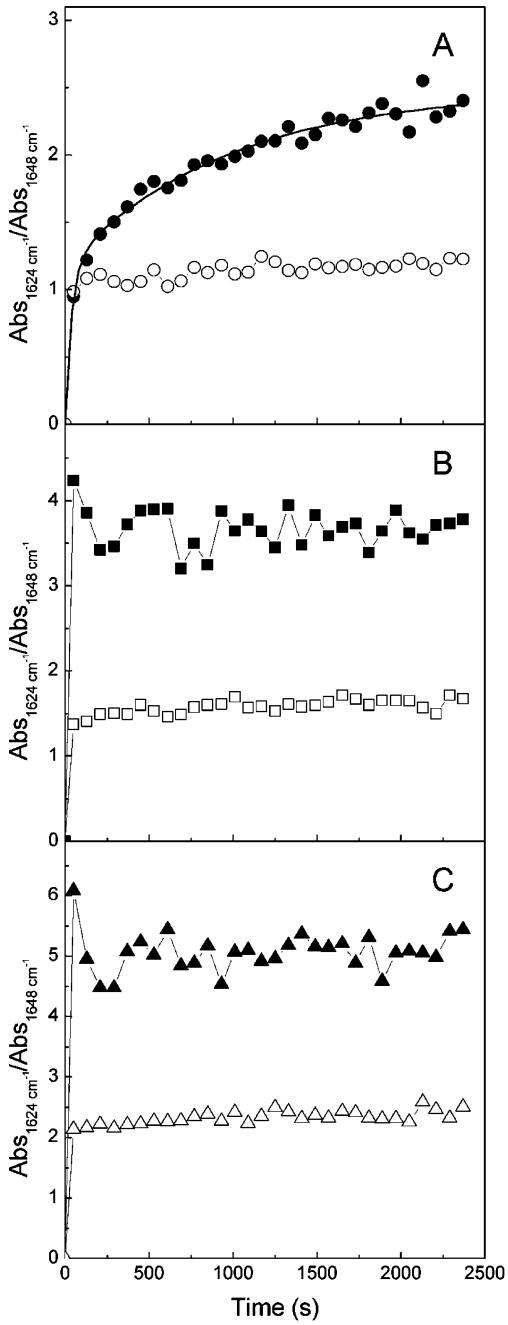

FIGURE 5: Kinetics of the structural changes illustrated in Figure 4. The formation of aggregated β structure from helical + unordered structures has been represented as the ratio of absorbances at 1624 and 1648 cm^{-1} versus time. (A) FP23-H, (B) FP23-Ac, and C (FP16). Full symbols: kinetics of the interactions of the peptides (1 mM) with PC/PE membranes, 10 mM lipid (L/P = 10). Hollow symbols: kinetics of the addition of the peptides into deuterated 10 mM Hepes buffer. Full circles in (A) were fitted to a double exponential function (eq 3). Each data point is the average of two independent measurements. Temperature 20 °C. pD 7.5.

(Figure 5A) the experimental points could be fitted to a double exponential function (eq 4), from which the apparent rate constants k_{app1} and k_{app2} were calculated (Table 1).

Figure 5B and Figure 5C clearly show that formation of the aggregated β structure when FP16 and FP23-Ac are mixed with the PC/PE vesicles is a rapid process that entirely falls within the dead time of the experimental procedure. The figure confirms that in all cases the amount of β structures formed with respect to other structures when the peptides are mixed with membranes is more than double the amount of β structure formed when the peptides are added into Hepes buffer.

Effect of Varying the Lipid/Peptide Ratio on the Rate Constants Derived from the FTIR Studies. One of the major problems when comparing kinetic data from structural studies (Figure 5) with data from "functional" studies (lipid mixing and binding data in this case, Figures 2 and 3) is the difference in the concentration required for each type of study. In the present work the peptide and lipid concentrations used in the FTIR studies reported in Figures 4 and 5 were 33 times higher than the concentrations used for the binding and lipid mixing experiments. To try to overcome this problem we have kept always constant the lipid peptide ratio (L/P = 10) for the measurements that had to be compared in kinetic terms. To properly sustain this approach we checked whether lowering the lipid and peptide concentrations but keeping constant the lipid/peptide ratio had any effect on the rate constant derived from the FTIR kinetic studies. Figure 6 shows the FTIR kinetics measured at the same lipid/peptide ratio as in Figure 5 for the FP23-H sequence (L/P = 10), but the lipid and the peptide concentrations being 10 times lower than that in Figure 5A. As described in the figure legend, the rate constants derived from the mathematical fit to eq 4 are very similar to those calculated from the data in Figure 5A and presented in Table 1. This experimental evidence allowed us to compare the kinetic constants derived from the structural and functional measurements (see next paragraph) and to be able to propose a general kinetic scheme in order to explain the data (see Discussion).

Comparison of the β Structure Formation, Membrane Binding, and Lipid Mixing Processes. To undertake a more detailed kinetic analysis of the different processes measured and described in the above sections, we proceeded to mathematically fit the experimental data (time traces) to exponential functions (eqs 3 and 4). The apparent rate constants derived from such fittings for the structural changes (formation of β structure), membrane binding, and lipid mixing processes reported in Figures 2−5 are summarized in Table 1 for the three peptidic sequences.

When the FP23-H peptide was mixed with the membranes, aggregated β structure formation data (Figure 5A, solid circles) fitted a double exponential process from which two apparent rate constants were calculated (Table 1): the first one (2.6×10^{-2} s^{-1}) is consistent with the formation of aggregates in Hepes buffer illustrated in Figure 5A (hollow symbols); the second, slower process has an apparent rate constant of 1.03×10^{-3} s^{-1}, which coincides with the higher apparent rate constant of the binding process (2.5×10^{-3} s^{-1}, time trace reported in Figure 2A). The slower lipid mixing process (Figure 3A) gave an apparent rate constant of 1.87×10^{-4} s^{-1}, very similar to the lower rate constant of the binding process (4.2×10^{-4} s^{-1}). These slow FPE fluorescence changes might reflect the effect of membrane fusion on the fluorescence of the FPE dye including perhaps conformational rearrangements of the peptide on the membrane surface. It can be therefore concluded that the formation of the aggregated β structure takes place as the FP23-H peptide binds to the membranes and that the structural change is followed by the lipid mixing process.

Table 1: Apparent Rate Constants (k_{app}) Calculated from the Mathematical Fitting of the Time Traces Reported in Figures 2−5 (Binding, Structural Changes, and Lipid Mixing) to Exponential Functions (Eqs 3 and 4)[a]

	k_{app1}, k_{app2} (s^{-1})		
	binding	$\rightarrow \beta$[b]	lipid mixing
FP23-H	$2.5 \times 10^{-3} \pm 6 \times 10^{-5}$ $4.2 \times 10^{-4} \pm 7 \times 10^{-6}$	$2.6 \times 10^{-2} \pm 5 \times 10^{-3}$ $1.03 \times 10^{-3} \pm 1.5 \times 10^{-4}$	$1.87 \times 10^{-4} \pm 1.4 \times 10^{-6}$
FP16	$2 \times 10^{-2} \pm 10^{-3}$ $7.6 \times 10^{-3} \pm 2.5 \times 10^{-4}$	nd[c]	$5 \times 10^{-2} \pm 4 \times 10^{-3}$ $8.55 \times 10^{-3} \pm 1.46 \times 10^{-4}$
FP23-Ac	$10^{-1} \pm 6 \times 10^{-3}$ $3 \times 10^{-3} \pm 1.7 \times 10^{-4}$	nd[c]	$5 \times 10^{-2} \pm 2 \times 10^{-3}$ $6.25 \times 10^{-3} \pm 9.52 \times 10^{-5}$

[a] The errors shown are the standard deviations calculated by the fitting program. [b] Structural change: from helical + unordered structures into aggregated β structures. [c] Not determined; the structural change in the case of FP16 and FP23-Ac is very fast, and occurs within the dead time of the experimental procedure (50 s).

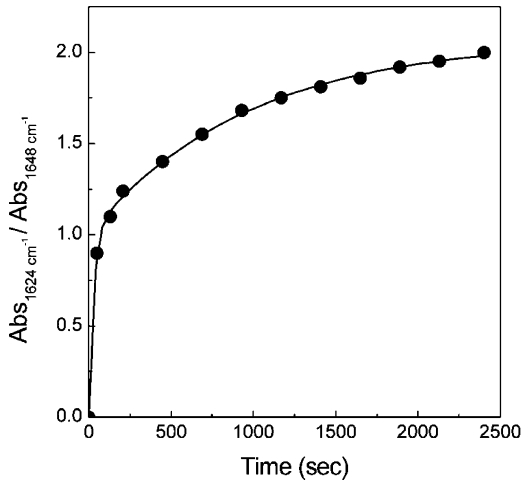

FIGURE 6: Kinetics of the structural change of FP23-H (0.1 mM peptide) when mixed with 1 mM lipid (L/P = 10). Data points were fitted to a double exponential function (eq 4). Rate constants derived form the mathematical fitting: $k_{app1} = 3.7 \times 10^{-2} \pm 3 \times 10^{-3}$ s $^{-1}$; $k_{app2} = 10^{-3} \pm 4 \times 10^{-5}$ s^{-1}. Conditions as in Figure 5.

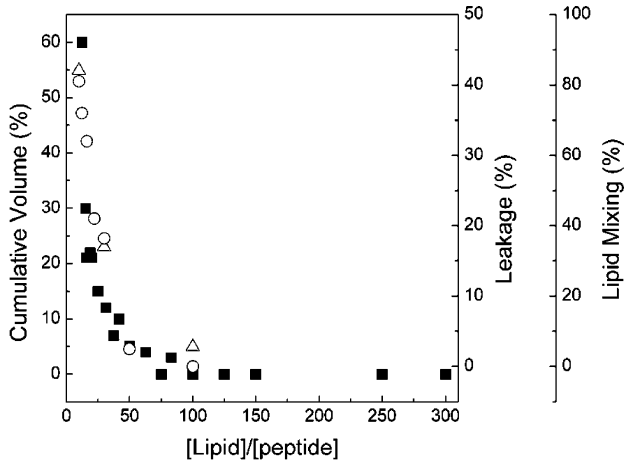

FIGURE 7: Changes in vesicle's size as a function of the lipid/peptide ratio (squares) compared to the percentage of vesicle leakage (triangles) and lipid mixing (circles) for FP16. Changes in size are expressed as percentage of cumulative volume, that is, as the percentage of the total vesicle's volume which corresponds to a population of particles with a diameter between 1 and 10 μm (diameter of the initial model vesicles is 100 nm). Conditions as in Figure 5.

No exponential curve could be fitted to the β structure formation data points corresponding to the FP23-Ac and FP16 sequences, reported in Figure 5, due to the lack of data between 0 and 50 s. Nevertheless, it can be safely concluded that the rate constant for the structural change would be smaller or at most equal to the rate constant calculated for the first of the two exponential processes to which the binding traces were fitted (2×10^{-2} and 10^{-1} s^{-1} in Table 1). So we can assume that also in this case the peptide molecules that bind to the membranes will form aggregated β structures as they bind. Moreover, for both FP23-Ac and FP16, the binding and lipid mixing processes fit a two exponential function that gave very similar apparent rate constants for both types of processes. Contrary to what has been said for FP23-H (lipid mixing is a process slower than binding), for the other two sequences, either lipid mixing takes place as the peptide binds and forms aggregated β structures or binding is the limiting step (lipid mixing being faster than binding).

Membrane Fusion, Vesicle Aggregation, and Leakage. In Figure 7 experimental data on membrane fusion, changes in the vesicle's size, and leakage of encapsulated ANTS/DPX, as a function of lipid/peptide ratio, are summarized for FP16. The same results were obtained for FP23-Ac and FP23-H (not shown). The figure indicates that, as the lipid/peptide ratio decreases, the percentage of a population of particles with diameters ranging from 1 to 10 μm with respect to the total vesicle volume increases. This can be interpreted as vesicle aggregation and is accompanied by membrane destabilization, which in turn causes leakage. This aggregation dependent leakage has been previously described (*58*).

Effect of Peptide Binding on the Hydration State of the Phospholipid Ester Carbonyl Group. To get some information on the effect of peptide binding on the lipid components we analyzed the lipid carbonyl infrared region (1700−1750 cm^{-1}), as shown in Figure 8 for the FP23-H sequence. According to what is described in the literature (*59*−*61*) the carbonyl band has two main components: a band centered at 1742 cm^{-1} which corresponds to the carbonyls which do not form hydrogen bonds with water molecules at the lipid water interface (dehydrated carbonyls) and another band centered at 1727 cm^{-1} corresponding to the carbonyls hydrogen bonded to water molecules (hydrated carbonyls). The same results were obtained for the other two peptides (FP16 and FP23-Ac). As it can be deduced from the curve-fittings reported in Figure 8, the interaction of the peptide clearly increases the intensity of the band assigned to the dehydrated carbonyls at the expense of the hydrated ones. Interaction of the peptide with the membranes would therefore have a dehydrating effect at the lipid water interface.

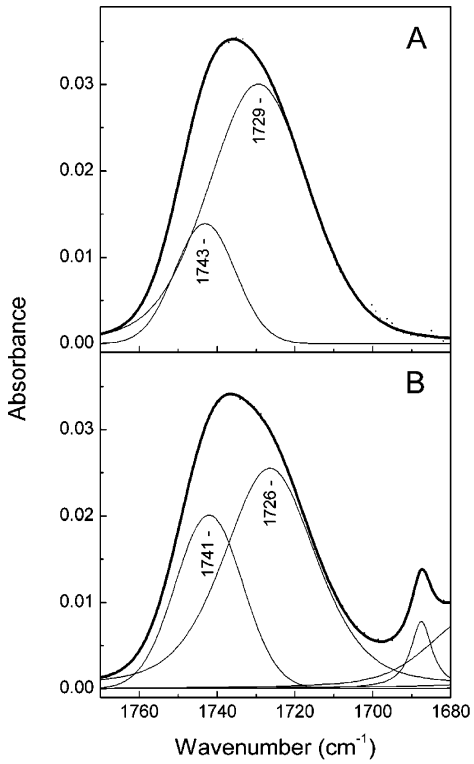

FIGURE 8: Esther carbonyl region of the FTIR spectra of PC/PE model membranes (A) and PC/PE model membranes mixed with the peptide FP23-H (B). Fitted Lorentzian component bands to the original infrared spectra using the Grams 3.2 (Galactic Inc.) program are shown. Experimental conditions as in Figure 5. Percentage area of component bands: in A, 1743 cm^{-1} (21%), 1729 cm^{-1} (79%); in B, 1741 cm^{-1} (34%), 1726 cm^{-1} (66%).

DISCUSSION

In spite of the great variety of studies on the interaction of the so-called HIV gp41 fusion peptides with membranes, a detailed description of the events that lead to membrane fusion is still lacking. Two important factors that make it difficult to summarize the existing corpus of data are, first, the fact that sequences differing in length (number of residues) and therefore in amino acidic composition have been used as model fusion peptides in different works, and second, the number of different experimental conditions, mainly in terms of the lipidic composition of the model membranes, in which the experiments have been carried out.

Whereas the fusogenic capacity of all the sequences described in the literature as gp41 fusion peptides has been quite unarguably established, this is not the case with respect to the peptidic structures which are responsible for destabilizing the membrane and triggering the fusion process. Obliquely inserted α helices and aggregated β structures are the two secondary structures that, depending on the study, have been described as the fusogenic structures (*21*−*33*, *40*).

In the present work it has been our aim to contribute to the resolution of the controversy with an approach based on two main strategies: (1) to compare the membrane interaction and lipid mixing capacity of the most widely used gp41 fusion peptide sequences (16 and 23 residues long) in exactly the same experimental conditions, in special a unique lipid composition; and (2) to study the conformational changes that the peptides undergo upon mixing with membranes, as a function of time. We followed this approach in order to overcome one of the shortages of the structural studies with fusion peptides in the past, that is, the fact that the structures described correspond to those present in the sample after the fusion process is completed.

On close examination of the literature, we realized that, for a detailed description of the sequence of events during the interaction of the fusion peptides with membranes, the first problem arises when we try to establish the conformation of the peptides in the solvent more commonly used to stock them in these cases, DMSO. Although Kliger et al. (*62*) state that they kept the peptide stocks in DMSO in order to avoid aggregation of the peptide prior to its use, no data has been reported, to our knowledge, illustrating it. Martin et al. (*25*) reported ATR-FTIR data which shows that the peptide, originally in DMSO, is heavily aggregated after being deposited on the ATR crystal and being exposed to a flux of dry air saturated with heavy water vapor. Such experimental conditions did probably result in a sample where the ratio DMSO/peptide was low compared to that in the initial peptide solution, due to the evaporation of the DMSO during the sample preparation process, which would explain the aggregation. Our FTIR spectra clearly show that the peptides in DMSO (a suspension at 1 mM peptide) are not aggregated (lack of the characteristic band around 1620 cm^{-1}). According to Jackson and Mantsch (*51*) it can be deduced that the peptides adopt an unordered structure, most probably due to the S═O groups in the DMSO molecule competing with the C═O groups in the peptidic bond to establish hydrogen bonds with the N−H in the amide.

Once the peptides are added from the DMSO solution to a membrane suspension, they interact with the membrane as the binding curves shown in Figure 2 prove. Binding curves for the 23 residue long fusion peptide have been previously reported using NBD-labeled peptides (*62*, *63*) but under experimental conditions very different from those of the present work. These authors do not observe any interaction of FP16 with lipidic membranes. In our case the binding curve measured for the FP16 sequence is consistent with the one reported before for this peptide by Cladera et al. (*64*). According to the results presented in Figure 2, the FP23-Ac binds to the membranes in a very similar way to that of FP16, that is, following a hyperbolic process with no sign of cooperativity. The most striking feature in the figure is the binding curve of FP23-H, the form with the protonated N-terminus (positively charged at neutral pH). In this case the binding curve profile is clearly sigmoidal. The Hill coefficient calculated from the mathematical fit to eq 2 is 9. That is a clear indication that, contrary to the interaction of FP16 and FP23-Ac, there are cooperative interactions between the FP23-H molecules upon membrane binding. Given the fact that gp41 exists as a trimer (*12*−*14*) and that membrane fusion seems to imply clustering of viral envelope glycoproteins on the surface of the target cell (*65*), it could be tempting to try to relate this particular Hill coefficient to the formation of 9-mers or trimers of trimers upon membrane binding. The fact that only FP23-H presents such a cooperative behavior, and not FP23-Ac nor FP16, could be related to a different solubility of the peptides in aqueous buffer. FTIR data shows that the three peptides rapidly aggregate into the buffer before interacting with the membrane. FP23-H is however less aggregated than FP23-Ac and much less than FP16 (Figure 4A,C,E). These conformational differences, reflecting the different solubility in water, could account for the observed differences in the binding kinetics and the

binding curves. At this point, it is convenient to bear in mind as well that Bentz and Mittal (*66*) reported that cooperative units derived from Hill plots for influenza hemagglutinin were not compatible with their proposed kinetic model. Given this discrepancy, we would consider it uncautious to stretch the interpretation of the Hill coefficient too far. An important outcome anyway from the results presented in Figure 2 is a quite distinctive behavior of the fusion peptide FP23 when the N-terminal residue is protonated. The oligomerization of FP23-H upon membrane binding is in agreement with the studies of Weliky and colleagues (*35*, *36*, *41*−*43*) using mainly nuclear magnetic resonance.

Such a difference between the interaction of FP23-H and that of the other two sequences is further illustrated by the lipid mixing measurements (Figure 3): lipid mixing is slower when triggered by FP23-H and a lower lipid/peptide ratio is sufficient for FP23-H in order to reach the same percentage of fusion, compared to FP16 and FP23-Ac, which follow very similar profiles.

Given the same experimental conditions, the results discussed above show that differences in membrane binding and lipid mixing do not depend on the length of the sequence, but rather on whether both ends of the sequence or only one bears a positive charge. That is, the different behavior does not depend on the protonation of the N-terminus (FP16 has a protonated N-ter as FP23-H) but on the total charge on the peptide sequence and possibly on the higher polarity of FP23-H.

The series of FTIR measurements on the variation of the peptidic secondary structure as a function of time (Figures 4 and 5) do contribute to further consolidate the differences between the interaction of FP23-H and the other two sequences, FP16 and FP23-Ac. When the N-terminus is in the amine form, a slow conformational change leading to the formation of aggregated β structures is detected. The kinetics of such a change could not be measured for the other two peptides, although as we shall discuss next, it is reasonable to think that the same conformational changes do take place, but faster. Let us first consider the FTIR spectra when the peptides are added into aqueous buffer (in the absence of membranes). The more hydrophobic the sequence, the more aggregated β structure forms in buffer (ordered from low to high β structure content: FP23-H < FP23-Ac < FP16, Figure 4A,C,E). Although the spectra of FP23-H point to the existence of oligomers in buffer (band at 1624 cm^{-1}, characteristic of intermolecularly hydrogen bonded structures), the aggregation band does not dominate the spectra, in which the band centered at 1648 cm^{-1} (mixture of helical and unordered structures) has approximately the same intensity. The relative intensity of this band with respect to the 1624 cm^{-1} one is clearly decreased for FP23-Ac (a sequence in which the segment 1−16 is more hydrophobic than in FP23-H due to the acetylation of the N-terminus) and has almost disappeared from the spectra of FP16, a peptide devoid of the more hydrophilic 17−23 segment.

If we compare now the FTIR spectra of the peptides in buffer with those in the presence of membranes, it is clear that the amount of β structure formed is higher when membranes are present for all the peptides (Figures 4 and 5) and the content in helical + unordered structures is reduced, for all the peptides as well, as compared to the content in buffer. Thus, membranes promote the formation of aggregated β structures.

For FP23-H, the following sequence of processes can be deduced from the comparison of the kinetics of β structure formation with those of membrane binding and membrane fusion (Figures 2−5 and Table 1):

$$FP_{DMSO} \rightarrow FP_{agw} \qquad (k_{app} \approx 10^{-2}\ s^{-1})$$

$$FP_{agw} + M \rightarrow FP_{\beta}\cdot M \qquad (k_{app} \approx 10^{-3}\ s^{-1})$$

$$2FP_{\beta}\cdot M \rightarrow FP_{\beta}\cdot M_F \qquad (k_{app} \approx 10^{-4}\ s^{-1})$$

where FP_{DMSO} is the fusion peptide dissolved in DMSO (unordered secondary structure), FP_{agw} is the fusion peptide forming β + helical + unordered structure aggregates in water, M is the membrane, $FP_{\beta}\cdot M$ is the complex formed when the aggregated peptide in water interacts with the membranes, and $FP_{\beta}\cdot M_F$ is the peptide−membrane complex after fusion has taken place. Fusion, therefore, is preceded by a conformational change which consists of the transformation of helical + unordered structures into β aggregated ones and such a conformational change takes place upon binding of the peptide to the membrane (coincidence of the second rate constant of the conformational change with the first rate constant of the binding process in Table 1).

According to the data in Table 1, FP23-Ac and FP16 present different kinetics compared to FP23-H. For these two sequences no rate constants could be derived for the conformational change (Figure 5B,C). It can be deduced however that it would be a process as fast as or faster than binding. On the other hand and contrary to the kinetics of FP23-H, the rate constants derived form binding and lipid mixing data for FP23-Ac and FP16 are very similar. This fact would be compatible with a kinetic model in which membrane binding was the limiting step (lipid mixing being faster than binding).

It is important to note that the kinetic analysis exposed above relies on the comparison of structural and functional data that has been obtained at quite different peptide concentrations. For this reason we have ensured that keeping constant the lipid/peptide ratio keeps unaltered the measured rate constant despite significantly changing both the peptide and the lipid concentrations (Figure 6). To explain this fact, it is useful to take into account that, upon binding of the peptide to the membrane surface, a reduction in dimensionality takes place (from the three dimensions in solution to the two dimensions on the membrane surface) as in the case of chemical reactions on a catalyst surface described in chemistry textbooks, where the velocity of the reaction depends on the concentration of the substance on the surface of the catalyst. According to such an approach, the peptide concentration on the membrane surface will remain unchanged while keeping constant the lipid/peptide ratio, that is in our case as long as L/P = 10 and therefore our structural and "functional" data (binding and lipid mixing) will be kinetically comparable.

Such a description of the kinetics of the binding and fusion processes together with that of the conformational changes involved is presented here for the first time. The resulting picture is in agreement with the fact, extensively described in previous works (*23*−*33*, *40*), that at lipid/peptide ratios at which fusion takes place, the dominant peptide structure is β aggregated. On the other hand, helical structures have been described to form at high lipid/peptide ratios (*23*−*33*,

40) or other nonfusogenic conditions. The occurrence of such structures is compatible with the spectroscopic FTIR band detected in our work at around 1648 cm^{-1}, early in the interaction of FP23-H with the model membranes, but also when the peptides (specially FP23-H) are dissolved in water.

The relevant fact is that, for the lipid mixing to take place, the peptides must undergo a conformational transition from helical + unordered into aggregated β structures, a transition which depends on the interaction with the membrane. On the other hand, this interaction with the membrane under fusogenic conditions implies a perturbation of the lipid−water interface, as the analysis of the FTIR spectra in the carbonyl region has shown (Figure 8). The interaction of the peptide would cause a certain degree of dehydration at the interface, a fact that would facilitate the fusion event. Such a dehydrating effect has been previously described for the N-terminal of the canine distemper virus fusion protein (*60*).

It is important to mention that formation of helical structures for the FP23 sequence at fusogenic lipid/peptide ratios has been described when the peptides' stock solutions are kept in HFIP (*67*, *68*). In this case, no formation of aggregated β is detected, but no data on the fusion capacity of the peptide dissolved in this solvent has been reported.

As Nir and Nieva (*58*) have pointed out, the fusion process must satisfy at least two requirements: (1) aggregation of the particles and a close apposition of the membranes and (2) a transitional destabilization of the bilayers. The data reported in the present paper (Figure 7) shows that vesicle aggregation and membrane destabilization (measured as vesicle leakage) both are effects concomitant to membrane fusion.

Finally we would like to point out that the importance of the protonation state of the N-terminal residue of the HIV fusion peptide evidenced in the present study should encourage future work directed to elucidate the protonation state in the native protein, since it is clear that this together with the role of other positive charges in the same fusion peptide (Arg22) or close to the fusion sequence (Arg31) can be an important factor in defining the molecular mechanism by which the virus enters the target cell.

ACKNOWLEDGMENT

We would like to thank Xavier León for his helpful assistance with the computer program for FTIR time-dependent measurements and Dr. Ramon Barnadas for his help using the ultrafine particle analyzer.

REFERENCES

1. Dutch, R. E., Jardetzky, T. S., and Lamb, R. A. (2000) Virus membrane fusion proteins: biological machines that undergo a metamorphosis, *Biosci. Rep. 20*, 597−612.
2. LeDuc, D. L., and Shin, Y. K. (2000) Insights into a structure-based mechanism of viral membrane fusion, *Biosci. Rep. 20*, 557−70.
3. Doms, R. W., and Moore, J. P. (2000) HIV-1 membrane fusion: targets of opportunity, *J. Cell Biol. 151*, F9−14.
4. Gallo, S. A., Finnegan, C. M., Viard, M., Raviv, Y., Dimitrov, A., Rawat, S. S., Puri, A., Durell, S., and Blumenthal, R. (2003) The HIV Env-mediated fusion reaction, *Biochim. Biophys. Acta 1614*, 36−50.
5. Gallo, S. A., Puri, A., and Blumenthal, R. (2001) HIV-1 gp41 six-helix bundle formation occurs rapidly after the engagement of gp120 by CXCR4 in the HIV-1 Env-mediated fusion process, *Biochemistry 40*, 12231−6.
6. Turner, B. G., and Summers, M. F. (1999) Structural biology of HIV, *J. Mol. Biol. 285*, 1−32.
7. Horvath, C. M., and Lamb, R. A. (1992) Studies on the fusion peptide of a paramyxovirus fusion glycoprotein: roles of conserved residues in cell fusion, *J. Virol. 66*, 2443−55.
8. Durell, S. R., Martin, I., Ruysschaert, J. M., Shai, Y., and Blumenthal, R. (1997) What studies of fusion peptides tell us about viral envelope glycoprotein-mediated membrane fusion (review), *Mol. Membr. Biol. 14*, 97−112.
9. Weissenhorn, W., Dessen, A., Calder, L. J., Harrison, S. C., Skehel, J. J., and Wiley, D. C. (1999) Structural basis for membrane fusion by enveloped viruses, *Mol. Membr. Biol. 16*, 3−9.
10. Freed, E. O., and Myers, D. J. (1992) Identification and characterization of fusion and processing domains of the human immunodeficiency virus type 2 envelope glycoprotein, *J. Virol. 66*, 5472−8.
11. Freed, E. O., Delwart, E. L., Buchschacher, G. L., Jr., and Panganiban, A. T. (1992) A mutation in the human immunodeficiency virus type 1 transmembrane glycoprotein gp41 dominantly interferes with fusion and infectivity, *Proc. Natl. Acad. Sci. U.S.A. 89*, 70−4.
12. Chan, D. C., Fass, D., Berger, J. M., and Kim, P. S. (1997) Core structure of gp41 from the HIV envelope glycoprotein, *Cell 89*, 263−73.
13. Tan, K., Liu, J., Wang, J., Shen, S., and Lu, M. (1997) Atomic structure of a thermostable subdomain of HIV-1 gp41, *Proc. Natl. Acad. Sci. U.S.A. 94*, 12303−8.
14. Weissenhorn, W., Dessen, A., Harrison, S. C., Skehel, J. J., and Wiley, D. C. (1997) Atomic structure of the ectodomain from HIV-1 gp41, *Nature 387*, 426−30.
15. Skehel, J. J., and Wiley, D. C. (2000) Receptor binding and membrane fusion in virus entry: the influenza hemagglutinin, *Annu. Rev. Biochem. 69*, 531−69.
16. Tamm, L. K. (2003) Hypothesis: spring-loaded boomerang mechanism of influenza hemagglutinin-mediated membrane fusion, *Biochim. Biophys. Acta 1614*, 14−23.
17. Tamm, L. K., Han, X., Li, Y., and Lai, A. L. (2002) Structure and function of membrane fusion peptides, *Biopolymers 66*, 249−60.
18. Tamm, L. K., and Han, X. (2000) Viral fusion peptides: a tool set to disrupt and connect biological membranes, *Biosci. Rep. 20*, 501−18.
19. Tatulian, S. A., and Tamm, L. K. (2000) Secondary structure, orientation, oligomerization, and lipid interactions of the transmembrane domain of influenza hemagglutinin, *Biochemistry 39*, 496−507.
20. Tatulian, S. A., Hinterdorfer, P., Baber, G., and Tamm, L. K. (1995) Influenza hemagglutinin assumes a tilted conformation during membrane fusion as determined by attenuated total reflection FTIR spectroscopy, *EMBO J. 14*, 5514−23.
21. Martin, I., Defrise-Quertain, F., Decroly, E., Vandenbranden, M., Brasseur, R., and Ruysschaert, J. M. (1993) Orientation and structure of the NH2-terminal HIV-1 gp41 peptide in fused and aggregated liposomes, *Biochim. Biophys. Acta 1145*, 124−33.
22. Martin, I., Defrise-Quertain, F., Mandieau, V., Nielsen, N. M., Saermark, T., Burny, A., Brasseur, R., Ruysschaert, J. M., and Vandenbranden, M. (1991) Fusogenic activity of SIV (simian immunodeficiency virus) peptides located in the GP32 NH2 terminal domain, *Biochem. Biophys. Res. Commun. 175*, 872−9.
23. Martin, I., Dubois, M. C., Defrise-Quertain, F., Saermark, T., Burny, A., Brasseur, R., and Ruysschaert, J. M. (1994) Correlation between fusogenicity of synthetic modified peptides corresponding to the NH2-terminal extremity of simian immunodeficiency virus gp32 and their mode of insertion into the lipid bilayer: an infrared spectroscopy study, *J. Virol. 68*, 1139−48.
24. Martin, I., Dubois, M. C., Saermark, T., Epand, R. M., and Ruysschaert, J. M. (1993) Lysophosphatidylcholine mediates the mode of insertion of the NH2-terminal SIV fusion peptide into the lipid bilayer, *FEBS Lett. 333*, 325−30.
25. Martin, I., Schaal, H., Scheid, A., and Ruysschaert, J. M. (1996) Lipid membrane fusion induced by the human immunodeficiency virus type 1 gp41 N-terminal extremity is determined by its orientation in the lipid bilayer, *J. Virol. 70*, 298−304.
26. Martin, I. I., Ruysschaert, J., and Epand, R. M. (1999) Role of the N-terminal peptides of viral envelope proteins in membrane fusion, *Adv. Drug Deliv. Rev. 38*, 233−55.
27. Pereira, F. B., Goni, F. M., Muga, A., and Nieva, J. L. (1997) Permeabilization and fusion of uncharged lipid vesicles induced

by the HIV-1 fusion peptide adopting an extended conformation: dose and sequence effects, *Biophys. J. 73*, 1977−86.
28. Pereira, F. B., Goni, F. M., and Nieva, J. L. (1995) Liposome destabilization induced by the HIV-1 fusion peptide effect of a single amino acid substitution, *FEBS Lett. 362*, 243−6.
29. Pereira, F. B., Goni, F. M., and Nieva, J. L. (1997) Membrane fusion induced by the HIV type 1 fusion peptide: modulation by factors affecting glycoprotein 41 activity and potential anti-HIV compounds, *AIDS Res. Hum. Retroviruses 13*, 1203−11.
30. Pereira, F. B., Valpuesta, J. M., Basanez, G., Goni, F. M., and Nieva, J. L. (1999) Interbilayer lipid mixing induced by the human immunodeficiency virus type-1 fusion peptide on large unilamellar vesicles: the nature of the nonlamellar intermediates, *Chem. Phys. Lipids 103*, 11−20.
31. Nieva, J. L., and Agirre, A. (2003) Are fusion peptides a good model to study viral cell fusion?, *Biochim. Biophys. Acta 1614*, 104−15.
32. Nieva, J. L., Nir, S., Muga, A., Goni, F. M., and Wilschut, J. (1994) Interaction of the HIV-1 fusion peptide with phospholipid vesicles: different structural requirements for fusion and leakage, *Biochemistry 33*, 3201−9.
33. Martin, I., and Ruysschaert, J. M. (2000) Common properties of fusion peptides from diverse systems, *Biosci. Rep. 20*, 483−500.
34. Maddox, M. W., and Longo, M. L. (2002) Conformational partitioning of the fusion peptide of HIV-1 gp41 and its structural analogs in bilayer membranes, *Biophys. J. 83*, 3088−96.
35. Yang, J., and Weliky, D. P. (2003) Solid-state nuclear magnetic resonance evidence for parallel and antiparallel strand arrangements in the membrane-associated HIV-1 fusion peptide, *Biochemistry 42*, 11879−90.
36. Yang, J., Parkanzky, P. D., Khunte, B. A., Canlas, C. G., Yang, R., Gabrys, C. M., and Weliky, D. P. (2001) Solid-state NMR measurements of conformation and conformational distributions in the membrane-bound HIV-1 fusion peptide. *J. Mol. Graphics Modell. 19*, 129−35.
37. Bradshaw, J. P., Darkes, M. J., Harroun, T. A., Katsaras, J., and Epand, R. M. (2000) Oblique membrane insertion of viral fusion peptide probed by neutron diffraction, *Biochemistry 39*, 6581−5.
38. Colotto, A., Martin, I., Ruysschaert, J. M., Sen, A., Hui, S. W., and Epand, R. M. (1996) Structural study of the interaction between the SIV fusion peptide and model membranes, *Biochemistry 35*, 980−9.
39. Colotto, A., and Epand, R. M. (1997) Structural study of the relationship between the rate of membrane fusion and the ability of the fusion peptide of influenza virus to perturb bilayers, *Biochemistry 36*, 7644−51.
40. Suarez, T., Gallaher, W. R., Agirre, A., Goni, F. M., and Nieva, J. L. (2000) Membrane interface-interacting sequences within the ectodomain of the human immunodeficiency virus type 1 envelope glycoprotein: putative role during viral fusion, *J. Virol. 74*, 8038−47.
41. Yang, J., Gabrys, C. M., and Weliky, D. P. (2001) Solid-state nuclear magnetic resonance evidence for an extended beta strand conformation of the membrane-bound HIV-1 fusion peptide, *Biochemistry 40*, 8126−37.
42. Yang, J., Prorok, M., Castellino, F. J., and Weliky, D. P. (2004) Oligomeric beta-structure of the membrane-bound HIV-1 fusion peptide formed from soluble monomers, *Biophys. J. 87*, 1951−63.
43. Yang, R., Yang, J., and Weliky, D. P. (2003) Synthesis, enhanced fusogenicity, and solid-state NMR measurements of cross-linked HIV-1 fusion peptides, *Biochemistry 42*, 3527−35.
44. Aloia, R. C., Tian, H., and Jensen, F. C. (1993) Lipid composition and fluidity of the human immunodeficiency virus envelope and host cell plasma membranes, *Proc. Natl. Acad. Sci. U.S.A. 90*, 5181−5.
45. Mayer, L. D., Hope, M. J., and Cullis, P. R. (1986) Vesicles of variable sizes produced by a rapid extrusion procedure. *Biochim. Biophys. Acta 858*, 161−8.
46. Wall, J., Ayoub, F., and O'Shea, P. (1995) Interactions of macromolecules with the mammalian cell surface, *J. Cell Sci. 108* (Part 7), 2673−82.
47. Golding, C., Senior, S., Wilson, M. T., and O'Shea, P. (1996) Time resolution of binding and membrane insertion of a mitochondrial signal peptide: correlation with structural changes and evidence for cooperativity, *Biochemistry 35*, 10931−7.
48. Struck, D. K., Hoekstra, D., and Pagano, R. E. (1981) Use of resonance energy transfer to monitor membrane fusion, *Biochemistry 20*, 4093−9.
49. Ellens, H., Bentz, J., and Szoka, F. C. (1985) H^+- and Ca^{2+}-induced fusion and destabilization of liposomes, *Biochemistry 24*, 3099−106.
50. Barnadas Rodriguez, R., and Sabes Xamani, M. (2003) Liposomes prepared by high-pressure homogenizers, *Methods Enzymol. 367*, 28−46.
51. Jackson, M., and Mantsch, H. H. (1991) Beware of proteins in DMSO, *Biochim. Biophys. Acta 1078*, 231−5.
52. Cladera, J., and O'Shea, P. (2001) Generic Techniques for Fluorescence Measurements of Protein−Ligand Interactions; Real Time Kinetics and Spatial Imaging, in *Protein−Ligand Interactions: structure and spectroscopy* (Harding, S. E., and Chowdhry, B. Z., Eds.) pp 169−200, Oxford University Press, Oxford.
53. Wall, J., Golding, C. A., Van Veen, M., and O'Shea, P. (1995) The use of fluoresceinphosphatidylethanolamine (FPE) as a real-time probe for peptide-membrane interactions, *Mol. Membr. Biol. 12*, 183−92.
54. Cladera, J., Martin, I., and O'Shea, P. (2001) The fusion domain of HIV gp41 interacts specifically with heparan sulfate on the T-lymphocyte cell surface, *EMBO J. 20*, 19−26.
55. Byler, D. M., and Susi, H. (1986) Examination of the secondary structure of proteins by deconvolved FTIR spectra, *Biopolymers 25*, 469−87.
56. Schweitzer-Stenner, R., Eker, F., Perez, A., Griebenow, K., Cao, X., and Nafie, L. A. (2003) The structure of tri-proline in water probed by polarized Raman, Fourier transform infrared, vibrational circular dichroism, and electric ultraviolet circular dichroism spectroscopy, *Biopolymers 71*, 558−68.
57. Schweitzer-Stenner, R., Eker, F., Huang, Q., and Griebenow, K. (2001) Dihedral angles of trialanine in D2O determined by combining FTIR and polarized visible Raman spectroscopy, *J. Am. Chem. Soc. 123*, 9628−33.
58. Nir, S., and Nieva, J. L. (2000) Interactions of peptides with liposomes: pore formation and fusion, *Prog. Lipid Res. 39*, 181−206.
59. Saez-Cirion, A., and Nieva, J. L. (2002) Conformational transitions of membrane-bound HIV-1 fusion peptide, *Biochim. Biophys. Acta 1564*, 57−65.
60. Aranda, F. J., Teruel, J. A., and Ortiz, A. (2003) Interaction of a synthetic peptide corresponding to the N-terminus of canine distemper virus fusion protein with phospholipid vesicles: a biophysical study, *Biochim. Biophys. Acta 1618*, 51−8.
61. Mantsch, H. H., and McElhaney, R. N. (1991) Phospholipid phase transitions in model and biological membranes as studied by infrared spectroscopy, *Chem. Phys. Lipids 57*, 213−26.
62. Kliger, Y., Aharoni, A., Rapaport, D., Jones, P., Blumenthal, R., and Shai, Y. (1997) Fusion peptides derived from the HIV type 1 glycoprotein 41 associate within phospholipid membranes and inhibit cell-cell fusion. Structure-function study. *J. Biol. Chem. 272*, 13496−505.
63. Pritsker, M., Rucker, J., Hoffman, T. L., Doms, R. W., and Shai, Y. (1999) Effect of nonpolar substitutions of the conserved Phe11 in the fusion peptide of HIV-1 gp41 on its function, structure, and organization in membranes, *Biochemistry 38*, 11359−71.
64. Cladera, J., Martin, I., Ruysschaert, J. M., and O'Shea, P. (1999) Characterization of the sequence of interactions of the fusion domain of the simian immunodeficiency virus with membranes. Role of the membrane dipole potential, *J. Biol. Chem. 274*, 29951−9.
65. Ugolini, S., Mondor, I., and Sattentau, Q. J. (1999) HIV-1 attachment: another look, *Trends Microbiol. 7*, 144−9.
66. Bentz, J., and Mittal, A. (2003) Architecture of the influenza hemagglutinin membrane fusion site, *Biochim. Biophys. Acta 1614*, 24−35.
67. Mobley, P. W., Waring, A. J., Sherman, M. A., and Gordon, L. M. (1999) Membrane interactions of the synthetic N-terminal peptide of HIV-1 gp41 and its structural analogs, *Biochim. Biophys. Acta 1418*, 1−18.
68. Gordon, L. M., Mobley, P. W., Pilpa, R., Sherman, M. A., and Waring, A. J. (2002) Conformational mapping of the N-terminal peptide of HIV-1 gp41 in membrane environments using (13)C-enhanced Fourier transform infrared spectroscopy, *Biochim. Biophys. Acta 1559*, 96−120.

BI050382R